

# The behavior of the structure function by using the effective exponent at low- $x$

B.Rezaei\* and G.R.Boroun†

*Physics Department, Razi University, Kermanshah 67149, Iran*

(Dated: November 8, 2018)

An analytical solution of the QCD evolution equations for the singlet and gluon distribution is presented. We decouple DGLAP evolution equations into the initial conditions by using a Laplace transform method at  $N^nLO$  analysis. The relationship between the nonlinear behavior and color dipole model is considered based on an effective exponent behavior at low- $x$  values. We obtain the effective exponent at NLO analysis from the decoupled behavior of the distribution functions. The proton structure function compared with H1 data from the inclusive structure function  $F_2(x, Q^2)$  for  $x \leq 10^{-2}$  and  $5 \leq Q^2 \leq 250 \text{ GeV}^2$ .

## Contents

<b>1. Introduction</b>	1
<b>2. Formulism Decoupling DGLAP</b>	2
<b>3. Decoupling DGLAP+GLRMQ</b>	3
<b>4. Behavior of the distribution functions</b>	4
<b>5. Effective Intercepts</b>	6
<b>6. The behavior of the structure function</b>	6
<b>7. Conclusion</b>	7
<b>References</b>	7

## 1. INTRODUCTION

Parton distribution functions can be used as fundamental tools to extract the structure functions of proton in deep inelastic scattering (DIS) processes. DIS is characterised by  $Q^2$  and  $x$  where  $Q^2$  is the virtuality of the exchanged virtual photon and  $x$  is the fraction of proton momentum carried by the parton. These distributions are prescribed in Quantum Chromodynamics (QCD) and extracted by the DGLAP [1] evolution equations. The solutions of these evolution equations allows us to predict the gluon and sea quark distributions at low values of  $x$  for understanding the quark-gluon dynamics inside the nucleon. On the basis of the DGLAP evolution equations at low  $x$  it is known that the dominate source for distribution functions is the gluon density. It is expected that the gluon density can not grow forever due to Froissart bound at very low values of  $x$ . The

gluon density behavior tamed in this region due to the correlative interactions between gluons. This behavior for the gluon density is very important in calculations of various high energy processes, as it can be checked at the Large Hadron electron Collider (LHeC) where leads to beyond a TeV in center-of-mass energy [2].

The LHeC center of mass energy is 1.3 TeV where extends the kinematic ranges in  $x$  and  $Q^2$  by factors of  $\sim 20$  than those accessible at HERA. The DIS kinematics reaches  $\simeq 1 \text{ TeV}^2$  and  $\simeq 10^{-6}$  for  $Q^2$  and  $x$  respectively where in this region the gluon distribution has a non-linear behavior. Although the LHeC is designed for study Higgs boson and Top quark production and also the CFT-ADS correspondence in low  $x$  physics [3]. The structure functions at low  $x$  and their  $Q^2$  dependence are sensitive to the gluon saturation in the LHeC kinematic range, as the dynamics of gluon behavior is an interesting subject in this region.

Indeed the nonlinear behavior is important when  $3\pi\alpha_s G(x, Q^2) \geq Q^2 R^2$ , where  $R$  is the size of the target. In such a case we reach the region of high gluon density QCD which annihilation of gluons becomes important. The annihilation introduced by the vertex  $gluon+gluon \rightarrow gluon$  with the probability  $\alpha_s^2 G^2(x, Q^2) \gg \pi^2 Q^2 R^4$  [4]. In fact the gluon recombination terms lead to nonlinear corrections to the evolution equations. In this region, the number of gluons are large therefore gluon recombination is particularly important because the structure functions behavior depends on the precise knowledge of the gluon distribution behavior. These multiple gluon-gluon interactions provide nonlinear corrections to the linear DGLAP evolution equations. These nonlinear corrections to the DGLAP equations have been calculated by Gribov, Levin, Ryskin, Mueller and Qiu (GLR-MQ) [5]. The nonlinear GLR-MQ corrections tame the parton distributions behavior at sufficiently low  $x$ .

In recent years [6-7], the Regge-like behavior for the gluon density used in the GLR-MQ equation. The key ingredient is the gluon behavior in this region, especially the effect of screening on the Regee trajectory. In Ref.[8]

\*Electronic address: brezaei@razi.ac.ir

†Electronic address: grboroun@gmail.com; boroun@razi.ac.ir

the prediction for the general behavior of the gluon density was studied at leading order using GLR-MQ equation by used the Laplace transformation method. Indeed this behavior has to be tamed by screening effects. These leads to the reduction of the growth of parton distributions, which is called parton saturation. This saturation known by the saturation scale  $Q_s^2(x)$  where the nonlinear effects appear for  $Q^2 < Q_s^2$ , function  $Q_s$ - called saturation scale- was taken in the following form  $Q_s^2 = Q_0^2(\frac{x}{x_0})^{-\lambda}$ .  $Q_0$  and  $x_0$  are free parameters and exponent  $\lambda$  is a dynamical quantity. Here, we suggest decoupled analytical independent solutions of the NLO DGLAP equations for the gluon distribution and the singlet structure function. Therefore we concentrate on the nonlinear behavior by the saturation model based on the decoupled solutions.

In the present paper, we study the theoretical framework including the decoupled DGLAP equations solutions in Laplace space into effective intercept behavior. The paper is organized as follows. In Section 2, we review the QCD coupled DGLAP evolution equations and present analytical solutions for the decoupled DGLAP evolution equations for the parton distribution functions (PDFs) based on the Laplace transform method. In Section 3 we apply the nonlinear behavior to the decoupled DGLAP equations and introduce a transition to the saturation model at low- $x$  values. Section 4 is devoted to the results for the gluon distribution function and also the proton structure function. The effective intercepts into the behavior of the distribution functions are presented. The effective intercepts for HERA data are obtained in Section 5 in accordance with the decoupled solutions. The behavior of the structure function is compared with H1 data for  $x \leq 10^{-2}$  and  $5 \leq Q^2 \leq 250 \text{ GeV}^2$  into the effective intercept in Section 6. Finally we give our summary and conclusions in section 7.

## 2. FORMULISM DECOUPLING DGLAP

The study of linear DGLAP evolution equations by using a Laplace transform have a history and many applications [9], both for coupled as well as decoupled distribution functions. In Ref.[9], a general method has been derived for calculation the evolution of parton distribution functions within the Laplace transform method. The polarized DGLAP evolution equations and the unpolarized DGLAP equation for the QCD evolution of parton distribution functions demonstrated in Refs.[10-12].

Starting from the coupled DGLAP evolution equations by using the Laplace transform method. As the Laplace transform method is highly appropriate for decoupling of the evolution equations, since it does not require any assumption on the distribution dynamics and provides

a direct relation to the measurements at low and high  $x$  values. Thus, the DGLAP equations can be directly calculated as a convolution of the  $s$ -space with impact factors that encode the splitting functions in that process as we have

$$\frac{\partial f_s(s, t)}{\partial t} = \left( \sum_{n=1} a^n(t) \Phi_f^{(n)}(s) \right) f_s(s, t) + \left( \sum_{n=1} a^n(t) \Theta_f^{(n)}(s) \right) g(s, t), \quad (1)$$

$$\text{and} \quad \frac{\partial g(s, t)}{\partial t} = \left( \sum_{n=1} a^n(t) \Phi_g^{(n)}(s) \right) f_s(s, t) + \left( \sum_{n=1} a^n(t) \Theta_g^{(n)}(s) \right) g(s, t). \quad (2)$$

The running coupling constant in the high-loop corrections of above evolution equations is expressed entirely thorough the variable  $a(t)$  as  $a(t) = \frac{\alpha_s}{4\pi}$ . Note that we used the Laplace  $s$ -space of the splitting functions as they are given by  $\Phi_f(s) = \mathcal{L}[P_{qg}(x); s]$ ,  $\Phi_g(s) = \mathcal{L}[P_{gq}(x); s]$ ,  $\Theta_f(s) = \mathcal{L}[P_{qq}(x); s]$  and  $\Theta_g(s) = \mathcal{L}[P_{gg}(x); s]$ . The splitting functions  $P_{ij}^n$  are the LO and  $N^n$ LO Altarelli-Parisi splitting kernels at one and high loops corrections presented in [13-14] which satisfy the following expansion

$$P_{ij}(x, \alpha_s(Q^2)) = \frac{\alpha_s}{4\pi} P_{ij}^{\text{LO}}(x) + \left( \frac{\alpha_s}{4\pi} \right)^2 P_{ij}^{\text{NLO}}(x) + \left( \frac{\alpha_s}{4\pi} \right)^3 P_{ij}^{\text{NNLO}}(x) + \dots \quad (3)$$

The running coupling constant  $\alpha_s$  has the following forms in NLO up to NNLO respectively [15]

$$\alpha_s^{\text{NLO}} = \frac{4\pi}{\beta_0 t} \left[ 1 - \frac{\beta_1 \ln t}{\beta_0^2 t} \right], \quad (4)$$

and

$$\alpha_s^{\text{NNLO}} = \frac{4\pi}{\beta_0 t} \left[ 1 - \frac{\beta_1 \ln t}{\beta_0^2 t} + \frac{1}{(\beta_0 t)^2} \left[ \left( \frac{\beta_1}{\beta_0} \right)^2 (\ln^2 t - \ln t + 1) + \frac{\beta_2}{\beta_0} \right] \right]. \quad (5)$$

where  $\beta_0 = \frac{1}{3}(33 - 2N_f)$ ,  $\beta_1 = 102 - \frac{38}{3}N_f$  and  $\beta_2 = \frac{2857}{6} - \frac{6673}{18}N_f + \frac{325}{54}N_f^2$ . The variable  $t$  is defined as  $t = \ln(\frac{Q^2}{\Lambda^2})$  and  $\Lambda$  is the QCD cut- off parameter at each heavy quark mass threshold as we take the  $N_f = 4$  for  $m_c^2 < \mu^2 < m_b^2$ .

When referring to a decoupling between differential equations (Eqs.1-2), the Laplace transform method exhibits two second-order differential evolution equation for singlet and gluon distribution function separately. In  $s$ -space these equations have the following forms:

$$\begin{aligned}
\frac{\partial^2 g(s, t)}{\partial t^2} = & [-(\sum_{n=1} a^n(t)\Theta_g^{(n)}(s))\frac{\partial}{\partial t}(\frac{1}{(\sum_{n=1} a^n(t)\Theta_g^{(n)}(s))}) + \sum_{n=1} a^n(t)(\Phi_f^{(n)}(s) + \Phi_g^{(n)}(s))]\frac{\partial g(s, t)}{\partial t} \\
& + [\sum_{n=1} a^n(t)\Theta_g^{(n)}(s)\frac{\partial}{\partial t}(\frac{\sum_{n=1} a^n(t)\Phi_g^{(n)}(s)}{\sum_{n=1} a^n(t)\Theta_g^{(n)}(s)}) - \sum_{n=1} a^n(t)\Phi_f^{(n)}(s)\sum_{n=1} a^n(t)\Phi_g^{(n)}(s) \\
& + \sum_{n=1} a^n(t)\Theta_g^{(n)}(s)\sum_{n=1} a^n(t)\Theta_f^{(n)}(s)]g(s, t), \tag{6}
\end{aligned}$$

$$\begin{aligned}
\frac{\partial^2 f_s(s, t)}{\partial t^2} = & [-(\sum_{n=1} a^n(t)\Theta_f^{(n)}(s))\frac{\partial}{\partial t}(\frac{1}{(\sum_{n=1} a^n(t)\Theta_f^{(n)}(s))}) + \sum_{n=1} a^n(t)(\Phi_f^{(n)}(s) + \Phi_g^{(n)}(s))]\frac{\partial f_s(s, t)}{\partial t} \\
& + [\sum_{n=1} a^n(t)\Theta_f^{(n)}(s)\frac{\partial}{\partial t}(\frac{\sum_{n=1} a^n(t)\Phi_f^{(n)}(s)}{\sum_{n=1} a^n(t)\Theta_f^{(n)}(s)}) - \sum_{n=1} a^n(t)\Phi_f^{(n)}(s)\sum_{n=1} a^n(t)\Phi_g^{(n)}(s) \\
& + \sum_{n=1} a^n(t)\Theta_g^{(n)}(s)\sum_{n=1} a^n(t)\Theta_f^{(n)}(s)]f_s(s, t). \tag{7}
\end{aligned}$$

In order to find solutions for distribution functions  $G(x, t)$  and  $F_2^s(x, t)$  we consider the inverse Laplace transform of splitting functions in  $s$ -space. One can determine these functions, at any order correction in  $x$ -space, for the decoupled second order differential equations in terms of the initial distributions. Solving these equations and taking all the above considerations into account, we find

$$\frac{\partial^2 G(x, t)}{\partial t^2} = [Eg1] \otimes \frac{\partial G(x, t)}{\partial t} + [Eg2] \otimes G(x, t), \tag{8}$$

$$\frac{\partial^2 F_2^s(x, t)}{\partial t^2} = [Es1] \otimes \frac{\partial F_2^s(x, t)}{\partial t} + [Es2] \otimes F_2^s(x, t). \tag{9}$$

The inverse Laplace transform of brackets in Eqs.(6) and (7) are defined as kernels  $Egi$  and  $Esi$  ( $i=1$  and  $2$ ) respectively. We note that here we firstly refer to the  $\nu$ -space as  $Efi(\nu, t) \equiv \mathcal{L}^{-1}[[...]; \nu]$  ( $f = g, s$ ), then considering the  $\nu \equiv \ln(1/x)$  one can finally arrive decoupled solutions of the DGLAP evolution equations with respect to  $x$  and  $t$  (or  $Q^2$ ) variables. These results are completely general and give the LO up to high-order expressions for gluon and singlet distribution functions. Therefore the decoupled solutions clearly are dependence on the initial distributions  $G(x, Q_0^2)$  and derivative of  $G(x, Q_0^2) (= \frac{\partial G(x, Q^2)}{\partial \ln Q^2} |_{Q^2=Q_0^2})$  and also  $F_s(x, Q_0^2)$  and derivative of  $F_s(x, Q_0^2) (= \frac{\partial F_s(x, Q^2)}{\partial \ln Q^2} |_{Q^2=Q_0^2})$  completely separately.

### 3. DECOUPLING DGLAP+GLRMQ

When  $x$  is small, annihilation comes into play as gluon density increases in a phase space sell  $\Delta \ln \frac{1}{x} \Delta \ln Q^2$ . In a phase space, the number of partons increases through

gluon splitting and decreases through gluon recombination. This behavior for the singlet and gluon distribution functions has been derived by GLR-MQ [5] as the GLRMQ evolution equation in terms of the gluon distribution function can be expressed as

$$\begin{aligned}
\frac{\partial G(x, Q^2)}{\partial \ln Q^2} = & \frac{\partial G(x, Q^2)}{\partial \ln Q^2} |_{DGLAP} \\
& - \frac{81}{16} \frac{\alpha_s^2}{R^2 Q^2} \int_x^1 \frac{dy}{y} [G(y, Q^2)]^2, \tag{10}
\end{aligned}$$

$$\begin{aligned}
\frac{\partial F_2^s(x, Q^2)}{\partial \ln Q^2} = & \frac{\partial F_2^s(x, Q^2)}{\partial \ln Q^2} |_{DGLAP} \\
& - \frac{27\alpha_s^2}{160R^2 Q^2} [xg(x, Q^2)]^2 + G_{HT}(x, Q^2). \tag{11}
\end{aligned}$$

The first terms in the above equations are the usual linear DGLAP terms, and the second terms in Eqs.(10) and (11) control the strong growth by the linear terms. The higher dimensional gluon term  $G_{TH}$  where  $HT$  denotes a further term notified by Mueller and Qiu [5] is here assumed to be zero. Also the quark gluon emission diagrams due to there little importance in the gluon rich low- $x$  region neglected. Indeed the interaction of the second gluon, when it is situated just behind another one, is not need to count if we have taken into account the interaction of the first one. These nonlinear corrections can be control by parameter  $\kappa = (\frac{3\pi^2\alpha_s}{2Q^2} \times \frac{G(x, Q^2)}{\pi R^2})$ . It means that in a large kinematic region  $\kappa \geq 1$  for high gluon density QCD (hdQCD), we expect that the nonlinear corrections should be large and important for a description of the LHeC data.

Defining the Laplace transforms of the nonlinear terms in Eqs.(10) and (11), and using the convolution factors

in this transformation in  $s$ -space as we have:

$$\frac{\partial f_s(s, t)}{\partial t} = [Eq.1] - T(R, Q^2)g(s, t)^2, \quad (12)$$

$$\frac{\partial g(s, t)}{\partial t} = [Eq.2] - \frac{K(R, Q^2)}{s}g(s, t)^2. \quad (13)$$

where  $T(R, Q^2) = \frac{27\alpha_s^2}{160R^2Q^2}$  and  $K(R, Q^2) = \frac{81\alpha_s^2}{16R^2Q^2}$ . The value of  $R$  is the correlation radius between two interacting gluons. It is the order of the proton radius ( $R \simeq 5 \text{ GeV}^{-1}$ ), if the gluons are distributed through the whole of proton, or much smaller ( $R \simeq 2 \text{ GeV}^{-1}$ ) if gluons are concentrated in hot-spot within the proton. Below, we state some basic definitions and results concerning nonlinear differential equations and decoupling between them in  $s$ -space, which essentially correspond to two second order nonlinear differential equations in this region. By considering the variable changes  $\nu \equiv \ln(1/x)$  and  $\omega \equiv \ln(1/z)$ , one can rewrite the nonlinear terms into

the  $\nu$ -variable as

$$K(R, Q^2) = \int_0^\nu \hat{G}^2(\omega, Q^2) d\omega,$$

where  $\hat{G}^2(\nu) \equiv G^2(e^{-\nu})$  and the function  $\hat{G}$  in  $\nu$ -space is define by

$$\hat{G}(\nu, Q^2) \equiv \hat{G}(e^{-\nu}, Q^2).$$

In the  $\nu$  space, we have defined the Laplace transform  $\int \frac{dy}{y} [G(y, Q^2)]^2 \equiv \int dw [\hat{G}(w, Q^2)]^2 = \frac{1}{s} \mathcal{L}[(\hat{G}(\nu, Q^2))^2; s]$  to be  $\frac{1}{s} [g(s, Q^2)]^2$  in  $s$ -space. Therefore Eqs.(12) and (13) define the DGLAP+GLRMQ evolution equations in  $s$ -space.

Next, using the idea from Section 2, we can decoupled the nonlinear equations (12) and (13) into the second order differential equations.

---


$$\begin{aligned} \frac{\partial^2 g(s, t)}{\partial t^2} = & [Eq.6] - [(\sum_{n=1} a^n(t) \Theta_g^{(n)}(s)) \frac{\partial}{\partial t} (\frac{K(R, t)}{(\sum_{n=1} a^n(t) \Theta_g^{(n)}(s))}) - (\sum_{n=1} a^n(t) \Phi_f^{(n)}(s)) K(R, t)] \frac{g^2(s, t)}{s} \\ & - [(\sum_{n=1} a^n(t) \Theta_g^{(n)}(s)) T(R, t)] g^2(s, t) - \frac{K(R, t)}{s} \frac{\partial g^2(s, t)}{\partial t}, \end{aligned} \quad (14)$$

$$\begin{aligned} \frac{\partial^2 F(s, t)}{\partial t^2} = & [Eq.7] + \frac{5}{18} [-(\sum_{n=1} a^n(t) \Theta_f^{(n)}(s)) \frac{\partial}{\partial t} (\frac{T(R, t)}{(\sum_{n=1} a^n(t) \Theta_f^{(n)}(s))}) + (\sum_{n=1} a^n(t) \Phi_g^{(n)}(s)) T(R, t)] g^2(s, t) \\ & - [(\sum_{n=1} a^n(t) \Theta_f^{(n)}(s)) K(R, t)] \frac{g^2(s, t)}{s} - K(R, t) \frac{\partial g^2(s, t)}{\partial t}. \end{aligned} \quad (15)$$


---

The one- and two-loop splitting functions (LO and NLO) in  $s$ -space for the parton distributions have been known in Refs.[9] and [12] respectively. In  $x$ -space, authors in Refs.[13] and [14] presented the exact results as well as compact parameterizations for the splitting functions at small  $x$ . The results and various aspects of those have been discussed in Ref.[13].

#### 4. BEHAVIOR OF THE DISTRIBUTION FUNCTIONS

Our prediction at small- $x$  is a transition from the linear to the nonlinear regime where we expect to observe the saturation of the growth of the gluon and singlet densities in this region. At high order corrections the ladder gluons are coupled together. We observe that a transition to the triple-Pomeron vertex is occurred in the leading  $\ln k^2$  approximation than a simple Pomeron. Indeed the

nonlinear evolution equation is a crude approximation because of the double logarithmic limit. The high energy factorization formula is an approach beyond this limit, as the correct degrees of freedom are given by  $q\bar{q}$  colorless dipoles for high energy  $\gamma^*p$  scattering. This behavior is related to the dipole cross section  $\sigma(x, r)$  where  $r$  is the  $q\bar{q}$  dipole transverse separation. The dipole cross section is given by [20]

$$\sigma_{q\bar{q}} = \sigma_0 \mathcal{N}(x, \mathbf{r}), \quad (16)$$

where  $\sigma_0$  is a constant which assures unitarity of the proton structure function, and  $\mathcal{N}(x, \mathbf{r}) = 1 - \exp(-\frac{r^2}{4R_0^2})$  is the dipole scattering amplitude. Here,  $R_0$  denotes the saturation radius as  $R_0^2 = \frac{1}{G_{eV^2}}(x/x_0)^\lambda$ . The parameters of the model were found from a fit to the data with  $x < 10^{-2}$  as  $\sigma_0 = 23 \text{ mb}$ ,  $\lambda \simeq 0.3$  and  $x_0 = 3.10^{-4}$ .

The virtual photon-proton cross sections  $\sigma_T$  and  $\sigma_L$ , for the transverse and longitudinal polarized virtual photons

take the form

$$\sigma_{T,L} = \int d^2\mathbf{r} dz |\Psi_{T,L}(\mathbf{r}, z, Q^2)|^2 \sigma_{q\bar{q}}, \quad (17)$$

where  $\Psi_T$  and  $\Psi_L$  are the light-cone wave function and related to the proton structure function by the following form

$$F_2(x, Q^2) = \frac{Q^2}{4\pi^2\alpha_{em}}(\sigma_T + \sigma_L). \quad (18)$$

In order to show our results we computed the singlet and gluon distribution functions into the decoupled second order evolution equations. The initial conditions starts at  $Q_0^2 = 1 \text{ GeV}^2$  with  $\alpha_s(1 \text{ GeV}^2) = 0.49128$  and  $\alpha_s(M_z^2) = 0.12018$  at NLO analysis [16]. The power law behavior of the distribution functions is considered in the decoupled DGLAP evolution equations. In principle if we take  $F_2 \sim x^{-\lambda_s}$  and  $G \sim x^{-\lambda_g}$  then we might expect to determine  $\lambda_s$  and  $\lambda_g$ . The behavior of exponent  $\lambda_s$  at fixed  $Q^2$  should be determined from Eq.9 by the proton structure function extracted in Ref.[17].

As can be seen in Fig.1, these derivatives are independent of  $x$  when compared with H1 2001 data [18] within the experimental accuracy. In this figure we show  $\lambda_s$  calculated as a function of  $x$  for  $5 \leq Q^2 \leq 250 \text{ GeV}^2$  from H1 2013 data [17] and they are consistent with other result [19]. In order to test the validity of our obtained exponents, we introduce the averaged value  $\lambda_i$ , ( $i = s$  and  $g$ ) (denoted in the following by  $\langle \dots \rangle$ ) in this research. In Fig.2 we show the NLO results for the proton structure function as a function of  $\langle \lambda_s \rangle$  as compared with H1 collaboration data [17]. It is tempting, however, to explore the possibility of obtaining approximate behavior of the exponents themselves in the restricted color dipole model point (i.e.,  $x_0$ ) at least. In Figs.3-4, approximate behavior of the exponents are shown at around a saddle point. These behaviors are shown for  $|\Delta\lambda_i| = \lambda_i - \langle \lambda_i \rangle$ . As seen in these figures, when  $Q^2$  increase, the saddle point is almost constant and it has the same behavior as observed for the color dipole model point.

Now let us discuss the choice of the intercept fixed for distribution functions where the small- $x$  behavior could well be more singular. We note that the behavior of the distribution functions with a  $Q^2$  independent value for intercept is controlled by a singularity factor in the complex angular momentum plane. For each  $Q^2$ , there is a cross-over point for the singlet and gluon intercepts at  $x = x_0$ . The low- $x$  behavior of the both gluon and sea quarks is controlled by the pomeron intercept. We therefore expect to have the intercepts for  $x < x_0$  and  $x > x_0$ , where the averaged value is taken as a constant factor throughout the calculation.

The results of the average to data are collected in Tables I and II for  $x < x_0$  and  $x > x_0$  respectively. In these tables a transition from the soft pomeron to the hard pomeron

intercept for distributions observed as  $Q^2$  increase. In Fig.5 we show  $\langle \lambda_i^j \rangle$  obtained for singlet structure function and gluon distribution function and compared with  $\lambda = \lambda_{phn}(Q^2)$  parameterized [21] where  $j = 1$  and 2 refer to  $x < x_0$  and  $x > x_0$ . In Ref.21, a phenomenologically exponent has been derived for calculating the evolution of singlet density for combined HERA  $e^+p$  DIS data [22] within the saturation model. With this method the low- $x$  behavior of the  $F_2$  structure function has been shown that  $F_2(x, Q^2) \sim x^{-\lambda_{phn}(Q^2)}$ , where  $\lambda_{phn}(Q^2)$  can be parameterized as  $\lambda_{phn}(Q^2) = 0.329 + 0.1 \log(\frac{Q^2}{90})$ .

In Fig.5 we observe that a linear behavior at low- $Q^2$  values and almost constant at high- $Q^2$  for exponents  $\langle \lambda_s \rangle$  is dominant. This clearly shows that the exponent  $\lambda_s$  has a different behavior in accordance with the critical point  $x_0$ . We also added results for the gluon exponent at low and high  $Q^2$  values in the same figure. Similar remarks apply to the gluon exponent where the scale of the exponent has been fixed at hard pomeron.

One can see that exponents obtained for gluon distribution function from the decoupled evolution equations are larger than the singlet exponent, that is  $\lambda_g > \lambda_s$ . Indeed the steep behavior of the gluon generates a similar steep behavior of singlet at small- $x$  where  $\lambda_s = \lambda_g - \epsilon$  in NLO analysis. Furthermore, the exact solution of the decoupled evolution equations predicts that  $\lambda_s$  and  $\lambda_g$  to be separate free parameters and the differences between these exponents are consistent to pQCD. In Fig.6 we show comparison of  $\Delta\lambda^j$  obtained using an averaged value between singlet and gluon distribution function. This  $\Delta\lambda^j$  shows that a scaling behavior property is exhibited for  $Q^2 > 5 \text{ GeV}^2$ . Note, that this scaling for singlet and gluon exponents in Fig.5 is clear at moderate and large  $Q^2$  values.

In Figures 7 and 8 we present the results for the proton structure function and the gluon distribution function at NLO analysis using the effective exponents respectively. We compare our results with those obtained by GJR parameterizations [23] and H1 2013 experimental data [17] in Fig.7. We use the range  $10^{-7} < x < 10^{-1}$  and  $5 \leq Q^2 \leq 250 \text{ GeV}^2$  to compare our results with H1 data at moderate  $x$ -range and other parameterizations at low- $x$  values based on the effective exponent behavior. In Fig.8 the gluon distribution behavior is compared with GJR parameterization with respect to the effective exponent behavior, as  $\langle \lambda_g \rangle$  is an averaged value of  $\lambda_g$  over  $x$ -range and other exponents obtained corresponding to  $x_0$ . The connection between the averaged value of exponent with effective exponent and color dipole model size is given in next sections.

## 5. EFFECTIVE INTERCEPTS

Perturbative QCD predicts a strong power-law rise of the gluon and singlet distribution at low  $x$ . This behavior coming from resummation of large powers of  $\alpha_s \ln 1/x$  where it is achieved by the use of the  $k_T$  factorization formalism which leads to the unintegrated gluon distribution rising as a power of  $x$ . This result is given in terms of the BFKL evolution equation as  $f(x, k_T^2) \sim x^{-\lambda}$  [20]. The function  $f(x, k_T^2)$  is the unintegrated gluon distribution and related to the gluon distribution from the DGLAP evolution equation by integration over the transverse momentum as  $G(x, Q^2) = \int^{Q^2} \frac{dk_T^2}{k_T^2} f(x, k_T^2)$ . One finds  $\lambda = 0.437$  where it is the so-called hard-Pomeron intercept. For comparing with the experimental data an effective intercept  $\lambda \simeq 0.3$  exhibited [20-21]. The strong rise into the  $k_T$  factorization formula is also true for the singlet structure function. The BFKL Pomeron does not depend on  $Q^2$ , however the effective Pomeron is  $Q^2$ -dependent when structure functions fitted to the experimental data at low values of  $x$ . This behavior can violate unitarity, so it has to be tamed by screening effects.

Indeed the nonlinear terms reduce the growth of singlet and gluon distributions at low- $x$ . The transition point for gluon saturation is given by the saturation scale  $Q_s^2 = Q_0^2 (\frac{x}{x_0})^{-\lambda}$  which is the  $x$ -dependent and this is an intrinsic characteristic of a dense gluon system. Here, we take into account the effects of kinematics which these are shown results a shift from the pomeron intercept to the effective intercept. This is related to fact that at low  $x$  we needed to produce the color dipole model in the argument of the gluon distribution as it can be computed from the  $k_T$  factorization formula [24]. We note that the nonlinear effects are small for  $Q^2 > Q_s^2$ , but very strong for  $Q^2 < Q_s^2$  where leading to the saturation of the scattering amplitude. These two regions separated by the saturation line,  $Q^2 = Q_s^2$ . When  $x \rightarrow x_0$ , we have  $Q^2 = Q_s^2 \rightarrow 1$  and this line is independent of  $\lambda$ -exponent. With respect to the averaged values of  $\lambda_s^1$  and  $\lambda_s^2$ , the relation  $Q^2 > Q_s^2$  is satisfied always when we used the HERA kinematical region for  $5 \leq Q^2 \leq 250 \text{ GeV}^2$  and  $10^{-6} \leq x \leq 10^{-2}$ . However we do not observe the nonlinear behavior with respect to these exponents defined. In Tables III and IV, we show some of parameters determined for the saturation behavior of the singlet structure function. These saturation parameters are obtained at  $Q^2 = 5 \text{ GeV}^2$  and  $250 \text{ GeV}^2$  respectively, as the averaged value of exponents  $\langle \lambda_i^j \rangle$  are taken account from Table I and II. In Tables III and IV, the saturation radius is defined in the form  $R_0^2(x) = \frac{1}{Q_0^2} (\frac{x}{x_0})^\lambda$  where  $Q_0^2 = 1 \text{ GeV}^2$  and the dimensionless variable  $\tau$  was postulated in the simplest form  $\tau = Q^2 R_0^2(x)$  [20]. The variable  $r$  denotes the separation between the quark and antiquark in color dipole model. This transverse dimension of the  $q\bar{q}$  pair

is small when the condition  $r < \frac{1}{Q}$  is fulfilled and large when  $r > \frac{1}{Q}$ . Indeed if  $r < r_s(x)$  the dipole cross section increase as  $x$  decreases. In Fig.9 we analyse the ratio of the dipole cross section,  $\sigma/\sigma_0$ , for different dimensionless variable  $\tau$ .

To better illustrate nonlinear effects at  $Q^2 < Q_s^2$ , we average over the exponents for  $5 \leq Q^2 \leq 250 \text{ GeV}^2$  presented in Tables I and II. As optimal values of parameters  $\lambda_s$  and  $\lambda_g$  we take  $\lambda_{ave}$  over the two different regimes as we have

$$\langle \lambda_s \rangle = 0.295 \quad \text{for } x < x_0 \quad \text{and} \quad 0.358 \quad \text{for } x > x_0,$$

$$\langle \lambda_g \rangle = 0.362 \quad \text{for } x < x_0 \quad \text{and} \quad 0.485 \quad \text{for } x > x_0.$$

Hence the averaged value to all exponents has the effective constraint as we obtained

$$\lambda_s^{eff} = 0.327 \quad \text{and} \quad \lambda_g^{eff} = 0.424. \quad (19)$$

One can see that the averaged exponents obtained for singlet and gluon distributions are closer to those defined by color dipole model and hard-pomeron exponents. In Ref.[21], authors have shown that the inclusive DIS value of singlet exponent is defined as  $\lambda_{inc} = 0.298 \pm 0.011$ , for combined HERA DIS data where errors are purely statistical. This parameter is defined to be 0.29 in GBW model [20] and it is an effective intercept in BFKL kernel. Also  $\lambda_g$  is comparable with the so-called hard Pomeron intercept [25]. Now the saturation condition  $Q^2 < Q_s^2$  is visible for low  $x$  values at low and moderate  $Q^2$  values. As illustrated in Fig.10 the transition occurs for decreasing transverse sizes at very low  $x$  values. Therefore these intercepts (Eq.19) guarantees consistency low  $x - Q^2$  behavior with saturation effects. The proton structure function behavior with respect to this effective exponent will study in next section.

## 6. THE BEHAVIOR OF THE STRUCTURE FUNCTION

In order to show the saturation effects at low values of  $x$ , we computed the proton structure function by the effective exponent obtained in Eq.19. In Fig.11 the  $F_2$  structure function is plotted as a function of  $x$  in bins of  $Q^2$  at NLO analysis. We compare our results with H1 experimental data [17-19,22]. The agreement between the experimental data and our calculation at moderate- $Q^2$  values is good, as the exponent value  $\lambda \sim 0.33$  is served for inclusive DIS and other methods. The regions where the results differ are the regions of low and high  $Q^2$ , where the effective exponent has to be smaller and larger than one obtained for decoupled distributions respectively. Notice that this behavior for

the exponent is closer than to the linear behavior with  $\ln Q^2$  as given in Ref.21. Indeed this behavior depends on fixed parameter  $x_0$  which we constrain analyzing for  $Q_s$ . In Fig.11 this prediction obtained at very low- $x$  values as the exponent is fixed in accordance with an effective intercept. In transition to the saturation model for low  $Q^2$ , one should take into account the quark mass, when we replace  $x \rightarrow (1 + \frac{4m_c^2}{Q^2})x$  in decoupled evolution equations [26]. Indeed one can modify  $\tau = \frac{Q^2}{Q_0^2}(\frac{x}{x_0})^\lambda$  to take into account  $m_c \simeq 1.3 \text{ GeV}^2$  and introduce scaling  $\tau_c = (1 + \frac{4m_c^2}{Q^2})\frac{Q^2}{Q_0^2}(\frac{x}{x_0})^\lambda$  [27]. However the transition to the low and high  $Q^2$  values is related to the regions that  $\lambda_s < \lambda_s^{eff} (\simeq 0.33)$  and  $\lambda_s > \lambda_s^{eff} (\simeq 0.33)$  respectively, as we observed that the effective pomeron is not a linear function into  $\ln Q^2$ . It has the nonlinear behavior with respect to the low and high  $Q^2$  values.

## 7. CONCLUSION

We presented the high-order decoupled analytical evolution equations for distribution functions, arising from the coupled DGLAP evolution equations. The Laplace transform technique used for the decoupled proton structure function and gluon distribution function evolution equations. Two homogeneous second-order differential evolution equations are obtained and extended to the nonlinear behavior at low- $x$  region. The next-to-leading -order analysis compared with H1 data with the averaged value of exponent  $\lambda_s$ . The averaged value of exponent  $\lambda_s$  has different behavior when the color dipole model is considered around the  $x_0$  value. The different between the gluon and singlet exponent considered at low- $x$  values and shown that they are the nonlinear function into  $\ln Q^2$  when used the new experimental data. The dipole cross section considered for nonlinear behavior at  $Q^2 < Q_s^2$ , as this behavior is very important for shown that the effective exponent with exact value is necessary for saturation effect. This effective exponent is basically the value of  $\simeq 0.33$  as reported in the literature. The proton structure function determined and compared with respect to this effective exponent for  $10^{-7} \leq x \leq 10^{-2}$  and  $5 \leq Q^2 \leq 250 \text{ GeV}^2$ .

## REFERENCES

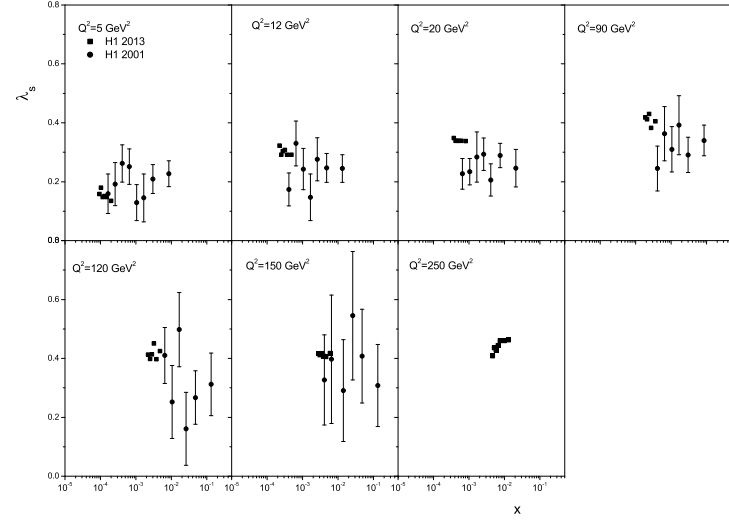
1. V. N. Gribov and L. N. Lipatov, Sov. J. Nucl. Phys. **15** (1972) 438; G. Altarelli and G. Parisi, Nucl. Phys. **B126** (1977) 298; Y. L. Dokshitzer, Sov. Phys. JETP **46** (1977) 641.
2. M. Klein, Ann. Phys. **528** (2016) 138.
3. P. Kostka et.al., Pos DIS2013 (2013) 256;
- L. Han et.al., Phys.Lett. **B771** (2017) 106; L. Han et.al., Phys.Lett. **B768** (2017) 241; Yao-Bei Liu, Nucl. Phys. **B923** (2017) 312.
4. E. Gotsman et.al., Nucl. Phys. **B539** (1999) 535; K. J. Eskola et.al., Nucl. Phys. **B660** (2003) 211.
5. L. V. Gribov, E. M. Levin and M. G. Ryskin, Phys. Rep. **100**, (1983) 1; A. H. Mueller and J. Qiu, Nucl. Phys. **B268** (1986) 427.
6. B. Rezaei and G. R. Boroun, Phys. Letts. **B692** (2010) 247; G. R. Boroun, Eur. Phys. J. **A42** (2009) 251; G. R. Boroun, Eur. Phys. J. **A43** (2010) 335.
7. P. Phukan et.al., arXiv:hep-ph/1705.06092; M. Lalung et.al., arXiv:hep-ph/1702.05291; M. Devee and J. K. sarma, Eur. Phys. J. **C74** (2014) 2751; M. Devee and J. K. sarma, Nucl. Phys. **B885** (2014) 571.
8. G. R. Boroun and S. Zarrin, Eur. Phys. J. Plus **128** (2013) 119; B. Rezaei and G. R. Boroun, Eur. Phys. J. **C73** (2013) 2412; G. R. Boroun and B. Rezaei, Eur. Phys. J. **C72** (2012) 2221.
9. Martin M. Block et al., Eur. Phys. J. **C69** (2010) 425; Phys. Rev. **D84** (2011) 094010; Phys. Rev. **D88** (2013) 014006.
10. F. Taghavi-Shahri et al., Eur. Phys. J. **C71** (2011) 1590.
11. H. Khanpour et al., Phys. Rev. **C95** (2017) 035201; S. Shoeibi et al., Phys. Rev. **D97** (2018) 074013.
12. H. Khanpour, A. Mirjalili and S. Atashbar Tehrani, Phys. Rev. **C95** (2017) 035201.
13. A. Vogt, S. Moch and J. A. M. Vermaseren, Nucl. Phys. **B691** (2004) 129.
14. C. D. White and R. S. Thorne, Eur. Phys. J. **C45** (2006) 179.
15. B. G. Shaikhatdenov, A. V. Kotikov, V. G. Krivokhizhin, G. Parente, Phys. Rev. **D81** (2010) 034008.
16. A. D. Martin, et al., Eur. Phys. J. **C63** (2009) 189.
17. V. Andreev et al. (H1 Collaboration), Eur. Phys. J. **C74** (2014) 2814.
18. C. Adloff et al. (H1 Collaboration), Eur. Phys. J. **C21** (2001) 33.
19. C. Adloff et al. (H1 Collaboration), Phys. Lett. **B520** (2001) 183.
20. K. Golec-Biernat and M. Wuesthoff, Phys. Rev. **D59** (1999) 014017; K. Golec-Biernat, Acta. Phys. Polon. **B33** (2002) 2771.
21. M. Praszalowicz and T. Stebel, JHEP **03** (2013) 090; T. Stebel, Phys. Rev. **D88** (2013) 014026.
22. F. D. Aaron et al. (H1 and ZEUS Collaboration), JHEP **1001** (2010) 109; Eur. Phys. J. **C63** (2009) 625; Eur. Phys. J. **C64** (2009) 561.
23. M. Gluk, P. Jimenez-Delgado and E. Reya, Eur. Phys. J. **C53** (2008) 355.
24. V. P. Goncalves and M. V. T. Machado, Phys. Rev. Lett. **91** (2003) 202002.
25. L. Motyka et al., arXiv:0809.4191v1 (2008); H. Kowalski et al., Eur. Phys. J. **C77** (2017) 777.

TABLE I: Averaged value of exponents for  $Q^2$  values at  $x < x_0$ .

$Q^2(GeV^2)$	$\langle \lambda_s^1 \rangle$	$\langle \lambda_g^1 \rangle$
5	0.135	0.307
12	0.262	0.336
20	0.295	0.353
90	0.337	0.376
120	0.342	0.385
150	0.344	0.387
250	0.351	0.391

TABLE II: The same as Table I but for  $x > x_0$ .

$Q^2(GeV^2)$	$\langle \lambda_s^2 \rangle$	$\langle \lambda_g^2 \rangle$
5	0.135	0.307
12	0.312	0.435
20	0.356	0.470
90	0.419	0.543
120	0.411	0.536
150	0.425	0.540
250	0.445	0.567



26. Z.Jalilian and G.R. Boroun, Phys.Lett. **B773**(2017)455.  
 27. E.Avsar and G.Gustafson, JHEP**0704** (2007) 067.

FIG. 1: The singlet exponent  $\lambda_s$ , from H1 2013 [17] compared with result H1 2001 [18-19], plotted against  $x$  at  $5 \leq Q^2 \leq 250 GeV^2$ .



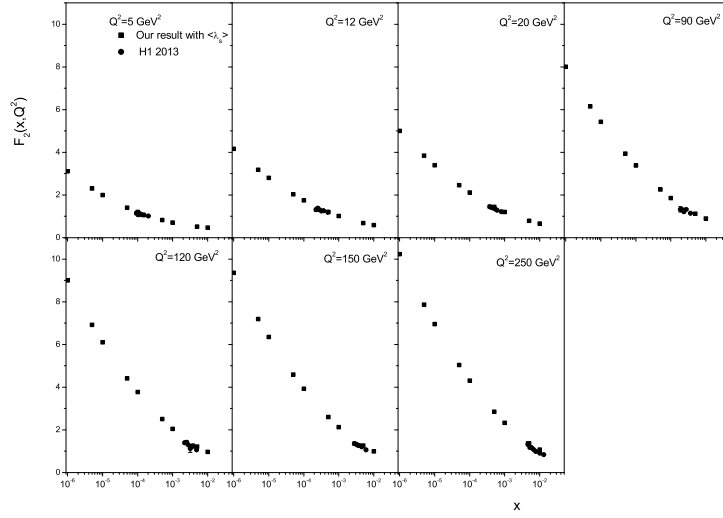


FIG. 2: The proton structure functions  $F_2(x, Q^2)$  with respect to  $\langle \lambda_s \rangle$  compared with H1 data [17] as accompanied with total errors.

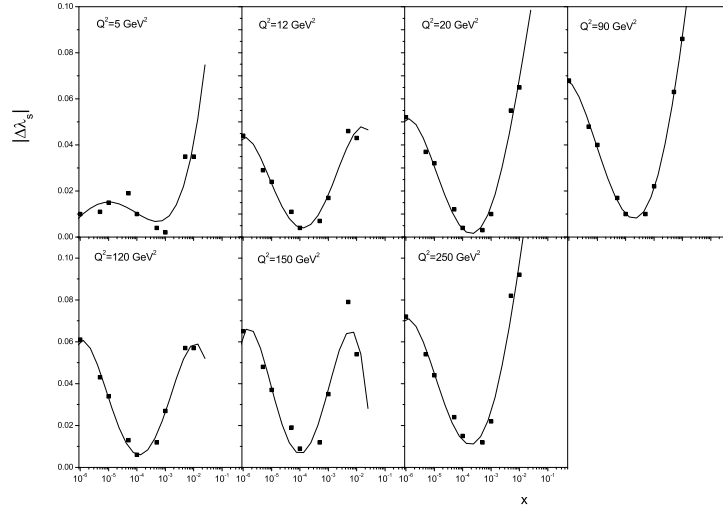


FIG. 3: The behavior of the singlet intercept,  $|\Delta\lambda_s|$ , for different energies obtained around  $x_0 \simeq 3.10^{-4}$ .

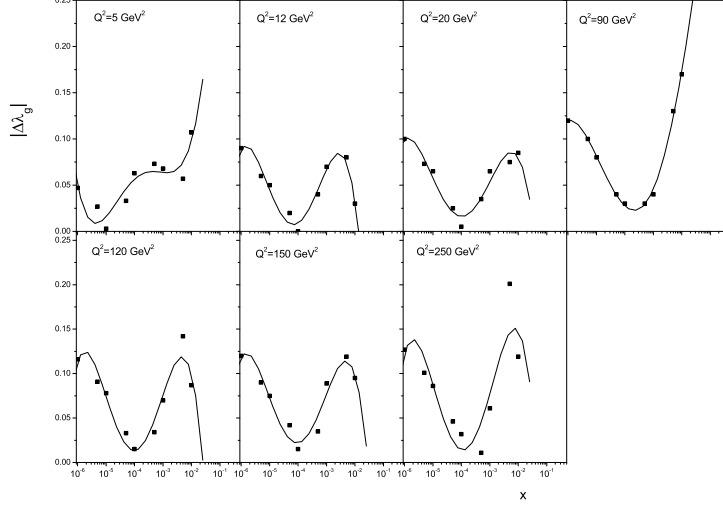


FIG. 4: The behavior of the gluon intercept,  $|\Delta\lambda_g|$ , for different energies obtained around  $x_0 \simeq 3.10^{-4}$ .

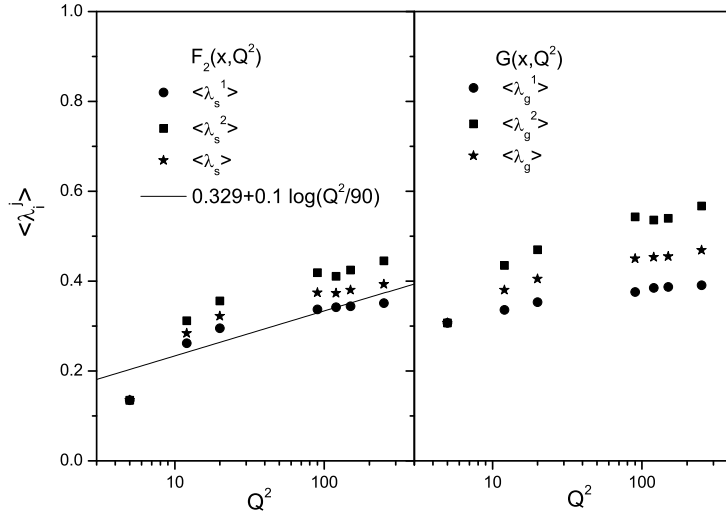


FIG. 5: Averaged value of singlet and gluon exponents with respect to the critical point as functions of  $Q^2$ . The linear fit is a effective exponent to H1 and ZEUS data in Refs.21-22.

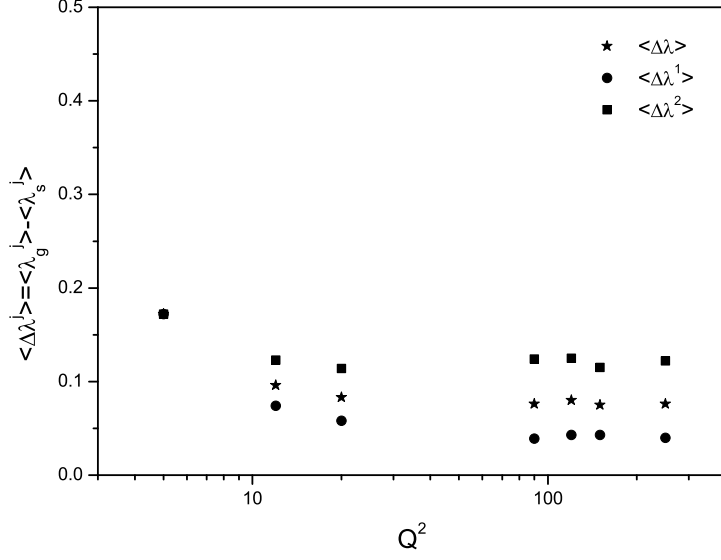


FIG. 6: Different of singlet and gluon exponents as functions of  $Q^2$ .

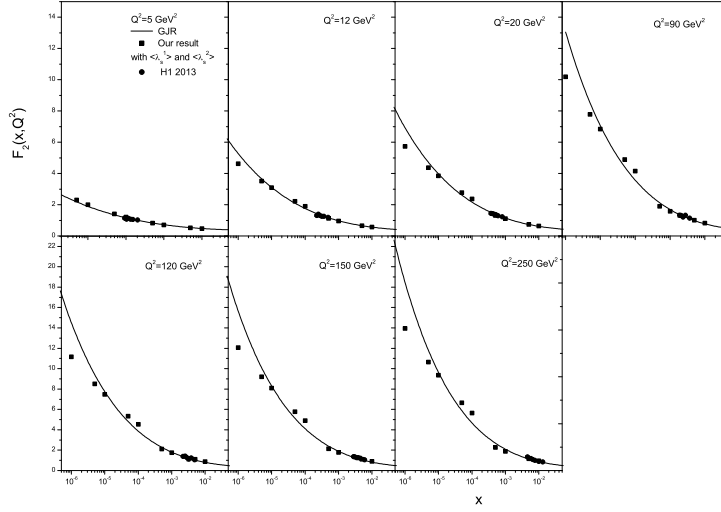


FIG. 7: The determined values of the structure function  $F_2(x, Q^2)$  plotted as functions of  $x$ , compared with H1 data [17] and GJR parameterization [23].

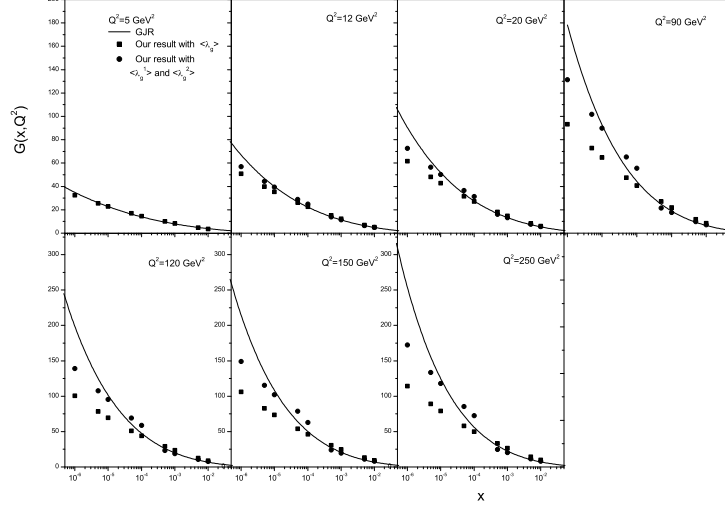


FIG. 8: The gluon distribution against  $x$  in a wide region of  $Q^2$  values compared with GJR parameterization [23].

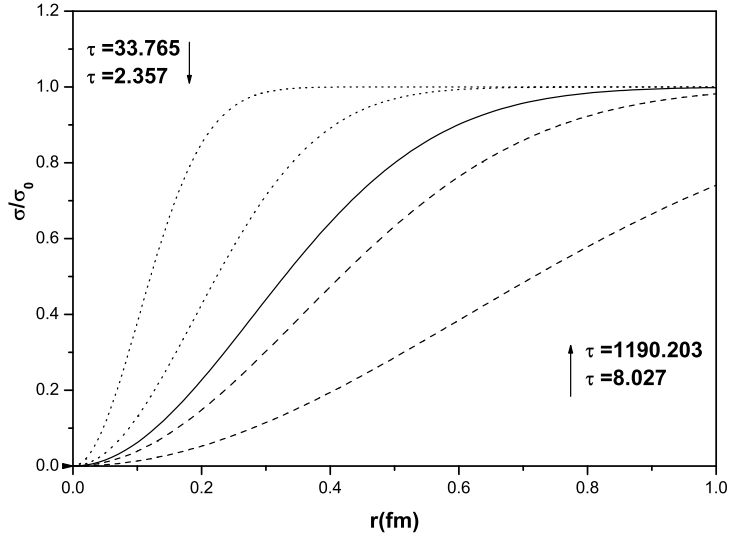


FIG. 9: The ratio of the dipole cross section with respect to the averaged exponents  $\langle \lambda_s^1 \rangle$  and  $\langle \lambda_s^2 \rangle$  for different values of  $\tau$ .

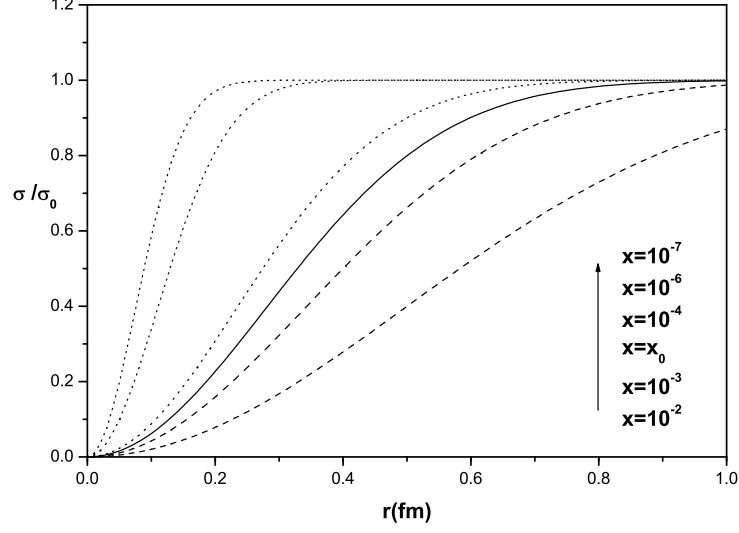


FIG. 10: The ratio of the dipole cross section with respect to the exponents  $\lambda_s^{eff} = 0.327$  for different values of  $x$  as the indicated dipole cross sections behavior change toward saturation at low- $r$ .

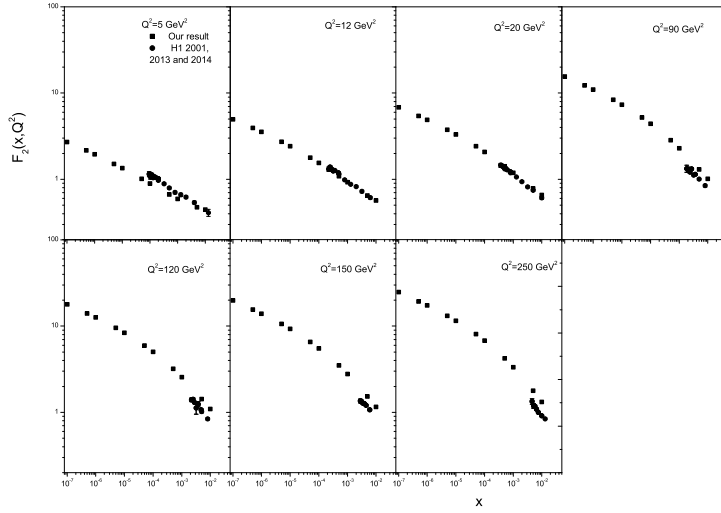


FIG. 11: Comparison of the proton structure function obtained from the decoupled evolution equation with the effective exponent to the H1 data collected since 2001 until 2014 [17-19,22].

TABLE III: Parameters determined at  $Q^2 = 5 \text{ GeV}^2$  for regions  $x < x_0$  and  $x > x_0$ .

$x$	$Q_{s1}^2(\text{GeV}^2)$	$Q_{s2}^2(\text{GeV}^2)$	$r_1(\text{GeV}^{-1})$	$r_2(\text{GeV}^{-1})$	$R_{01}^2(\text{GeV}^{-2})$	$R_{02}^2(\text{GeV}^{-2})$
1E-6	2.160	—	0.680	—	0.463	—
5E-6	1.738	—	0.758	—	0.575	—
1E-5	1.583	—	0.795	—	0.632	—
5E-5	1.274	—	0.886	—	0.785	—
1E-4	1.160	—	0.928	—	0.862	—
5E-4	—	0.934	—	1.035	—	1.071
1E-3	—	0.850	—	1.085	—	1.177
5E-3	—	0.684	—	1.209	—	1.462
1E-2	—	0.623	—	1.267	—	1.605

TABLE IV: The same as Table III but for  $Q^2 = 250 \text{ GeV}^2$ .

$x$	$Q_{s1}^2(\text{GeV}^2)$	$Q_{s2}^2(\text{GeV}^2)$	$r_1(\text{GeV}^{-1})$	$r_2(\text{GeV}^{-1})$	$R_{01}^2(\text{GeV}^{-2})$	$R_{02}^2(\text{GeV}^{-2})$
1E-6	7.404	—	0.367	—	0.135	—
5E-6	4.208	—	0.487	—	0.238	—
1E-5	3.300	—	0.550	—	0.303	—
5E-5	1.876	—	0.730	—	0.533	—
1E-4	1.470	—	0.825	—	0.680	—
5E-4	—	0.800	—	1.120	—	1.255
1E-3	—	0.585	—	1.307	—	1.709
5E-3	—	0.286	—	1.870	—	3.497
1E-2	—	0.210	—	2.182	—	4.761